Heliyon 10 (2024) e30411

Contents lists available at ScienceDirect

Heliyon

journal homepage: www.cell.com/heliyon

Research article

Predicting glioblastoma recurrence using multiparametric MR imaging of non-enhancing peritumoral regions at baseline

Zhen Xing [a,b,1], Cong Wang [c,1], Wen Yang [d], Dejun She [a,b], Xiefeng Yang [a,b], Dairong Cao [a,b,e,f,*]

[a] Department of Radiology, The First Affiliated Hospital, Fujian Medical University, Fuzhou, 350005, China
[b] Department of Radiology, National Regional Medical Center, Binhai Campus of the First Affiliated Hospital, Fujian Medical University, Fuzhou, 350212, Fujian, China
[c] Department of Nuclear Medicine, The First Affiliated Hospital, Fujian Medical University, Fuzhou, 350005, China
[d] The Webb Schools, Claremont, CA, 91711, USA
[e] Department of Radiology, Fujian Key Laboratory of Precision Medicine for Cancer, The First Affiliated Hospital, Fujian Medical University, Fuzhou, 350005, China
[f] Key Laboratory of Radiation Biology of Fujian Higher Education Institutions, The First Affiliated Hospital, Fujian Medical University, Fuzhou, 350005, China

ARTICLE INFO

Keywords:
Glioblastoma
Recurrence
Infiltration
T2-FLAIR
DWI
DSC-PWI

ABSTRACT

Background: To assess the feasibility of multiparametric magnetic resonance imaging in predicting tumor recurrence in nonenhancing peritumoral regions in patients with glioblastoma at baseline.
Methods: Fifty-eight patients with recurrent glioblastoma underwent multiparametric magnetic resonance imaging, including T2-weighted fluid-attenuated inversion recovery, diffusion-weighted imaging, and dynamic susceptibility contrast perfusion-weighted imaging. Non-enhancing peritumoral regions with glioblastoma recurrence were identified by coregistering preoperative and post-recurrent magnetic resonance images. Regions of interest were placed in nonenhancing peritumoral regions with and without tumor recurrence to calculate the apparent diffusion coefficient value, and relative ratios of T2-weighted fluid-attenuated inversion recovery signal intensity, apparent diffusion coefficient, and cerebral blood volume values.
Results: Significant lower relative T2-weighted fluid-attenuated inversion recovery signal intensity, apparent diffusion coefficient, and relative apparent diffusion coefficient but higher relative cerebral blood volume values were found in the nonenhancing peritumoral regions with tumor recurrence than without recurrence (all $P < 0.05$). The threshold values ≥ 0.89 for relative cerebral blood volume provide the optimal performance for predicting the nonenhancing peritumoral regions with future tumor recurrence, with the sensitivity, specificity, and accuracy of 84.7%, 83.6%, and 85.8%, respectively. The combination of relative T2-weighted fluid-attenuated inversion recovery signal intensity, apparent diffusion coefficient, and relative cerebral blood volume can provide better predictive performance than relative cerebral blood volume ($P = 0.015$).

* Corresponding author. Department of Radiology, First Affiliated Hospital of Fujian Medical University, 20 Cha-Zhong Road, Fuzhou, Fujian, 350005, China
E-mail address: dairongcao@163.com (D. Cao).
[1] **First author:** the first two authors contributed equally to this manuscript and should be the co-first authors.

https://doi.org/10.1016/j.heliyon.2024.e30411
Received 18 July 2023; Received in revised form 24 April 2024; Accepted 25 April 2024
Available online 26 April 2024

Conclusion: The combined use of T2-weighted fluid-attenuated inversion recovery, diffusion-weighted imaging, and dynamic susceptibility contrast perfusion-weighted imaging can effectively estimate the risk of future tumor recurrence at baseline.

List of abbreviations

GBM	Glioblastoma
MRI	Magnetic Resonance Imaging
ADC	Apparent Diffusion Coefficient
DWI	Diffusion-Weighted Imaging
FLAIR	Fluid-Attenuated Inversion Recovery
DSC-PWI	Dynamic Susceptibility Contrast Perfusion-Weighted Imaging
NEPTRs	Non-Enhancing Peritumoral Regions
WHO	World Health Organization
IDH	Isocitrate Dehydrogenase
TR	Time of Repetition
TE	Time of Echo
FOV	Field Of View
NEX	number of excitations
Gd-BOPTA	Gadobenate Dimeglumine
AIF	Arterial Inflow Effect
CBV	Cerebral Blood Volume
CBF	Cerebral Blood Flow
MTT	Mean Transit Time
ROIs	Regions Of Interest
ICC	Intraclass Correlation Coefficient
ROC	Receiver Operating Characteristic
AUC	Area Under the Curve

1. Introduction

Glioblastoma (GBM) stands as the most prevalent malignant brain tumor in adults, characterized by a median survival time of merely 18–24 months [1]. The current standard treatment for newly diagnosed GBM entails gross total surgical resection, accompanied by adjuvant radiotherapy alongside concomitant and adjuvant temozolomide [2,3]. Clinically, the primary objective of gross total resection is the contrast-enhancing and high-grade portion of the tumor as indicated by magnetic resonance imaging (MRI), which manifests a leaky blood-brain barrier [4]. However, GBM represents a diffusely infiltrating and widely spread malignant entity; hence, the margins of the contrast-enhancing region fail to accurately delineate the true tumor margins. This limitation potentially contributes to inevitable recurrence and treatment failure in GBM patients [5,6]. Therefore, the early identification of peritumoral areas at risk for future GBM recurrence on preoperative MR images assumes paramount importance for enabling preemptive intervention and enhancing patient prognosis [7].

Histopathological evidence indicates that GBM recurrence originates from residual non-enhancing infiltrative tumor cells that intermingle with peritumoral edema, persisting even immediately after surgical resection [8,9]. Previous studies have suggested that areas at risk for future GBM recurrence exhibit subtle variations in the apparent diffusion coefficient (ADC) values derived from diffusion-weighted imaging (DWI) and in signal intensity within the peritumoral region on T2-weighted and fluid-attenuated inversion recovery (FLAIR) images [10–13]. The utilization of multiparametric MRI, such as DWI and dynamic susceptibility contrast perfusion-weighted imaging (DSC-PWI), enables discrimination between infiltrating tumor cells and surrounding vasogenic edema or normal tissues [14,15]. However, prior studies have typically considered non-enhancing peritumoral regions (NEPTRs) in GBM as a whole, neglecting their high heterogeneous nature. Consequently, it remains unclear whether these potentially informative MR methods can accurately identify NEPTRs with a high risk of future GBM recurrence.

In this study, we evaluated distinct subregions of the NEPTRs in GBM individually, as proposed by Bette et al. [16], hypothesizing that multiparametric MRI findings in NEPTR subregions would significantly differ between areas with and without future local tumor recurrence. Accordingly, our objective was to determine whether future local tumor recurrence in NEPTR subregions could be predicted using baseline multiparametric MRI, including T2-FLAIR, DWI, and DSC-PWI, in patients with GBM.

2. Materials and methods

2.1. Patients

The retrospective study was approved by the ethics committee of our hospital, with a waiver of the requirement for patient informed consent. A total of 557 patients with GBM who underwent gross total surgical resection from October 2009 to December 2022 at our hospital were initially selected. Inclusion criteria comprised: (a) undergoing multiparametric MR examinations, including conventional MRI, DWI, and DSC-PWI, before any treatment; (b) post-operative MR examinations performed within 74 h or 2 weeks after resection to confirm the absence of residual contrast-enhancing lesions; (c) definitive histopathological diagnosis of GBM according to the World Health Organization (WHO) 2021 classification criteria; (d) follow-up MRIs demonstrating convincing evidence of tumor recurrence according to the updated Response Assessment in Neuro-Oncology criteria [17]; and (e) receiving radiation therapy and concurrent temozolomide treatment after gross total resection to minimize potential confounding effects from treatment protocol heterogeneity. Exclusion criteria included [1]: indeterminate enhancement lesions, such as pseudo-progression and/or radiation necrosis after treatment [2]; adjunctive or alternative chemotherapy (besides temozolomide) [3]; incomplete serial follow-up MRI in our hospital before GBM recurrence; and [4] inadequate quality of multiparametric MR images. MRI assessments were conducted by a neuroradiologist blinded to the results. Based on the criteria, cases before 2017 were excluded due to lack of isocitrate dehydrogenase (IDH) gene testing, resulting in 289 exclusions. Additionally, 35 patients were excluded for not undergoing multiparametric MR examinations, 5 for incomplete MRI post-surgery, 9 for non-tumor recurrence, and 18 for inability to receive concurrent radiotherapy and chemotherapy. Ultimately, 201 patients met the inclusion criteria. Further exclusions were made for pseudoprogression or radionecrosis (12 cases), incomplete MR follow-up (114 cases), bevacizumab treatment before recurrence (14 cases), and image quality issues (3 cases), resulting in a final inclusion of fifty-nine patients (37 men, 22 women; mean age ± standard deviation: 55.23 ± 13.21 years; age range: 31–75 years).

2.2. MR techniques

Images were acquired as part of routine clinical procedures using a 3.0 T MR imaging system (Magnetom Verio/Skyra TIM; Siemens Healthcare, Germany) equipped with an 8-channel head matrix coil. The imaging protocols included axial T1-weighted gradient-echo imaging (time of repetition [TR] = 250 msec; time of echo [TE] = 2.48 msec), axial T2-weighted turbo spin-echo imaging (TR = 4000 msec; TE = 96 msec), axial T2-FLAIR imaging (TR/TE, 9000/94 msec; inversion time, 2500 msec), and three orthogonal planes of contrast-enhanced gradient-echo T1-weighted imaging (CE-T1WI TR/TE, 250/2.48 msec) following DSC-PWI sequences. The imaging

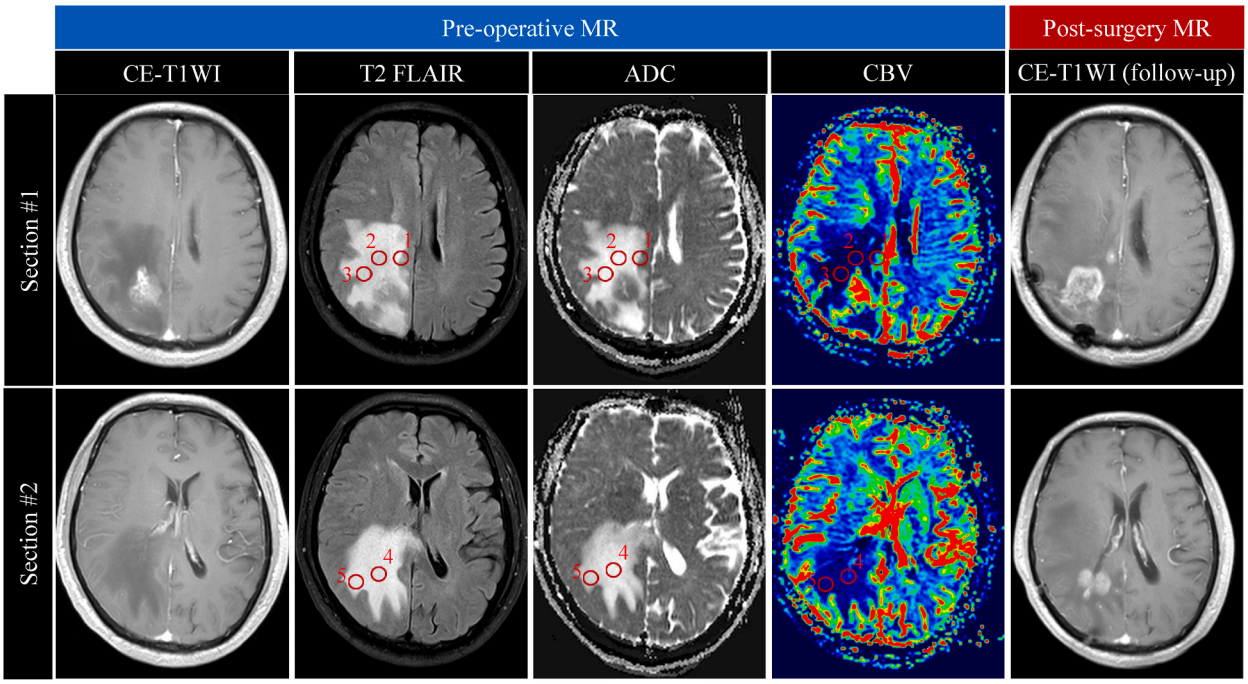

Fig. 1. The illustration demonstrates the placement of regions of interest (ROIs) within the nonenhancing peritumoral regions, utilizing coregistration techniques to align preoperative and post-surgery MR images. ROIs 1, 3, and 4 are situated within regions exhibiting future tumor recurrence, while ROIs 2 and 5 are positioned in regions devoid of future tumor recurrence. These placements are based on contrast-enhanced (CE)-T1WI, T2-weighted fluid-attenuated inversion recovery (T2-FLAIR), apparent diffusion coefficient (ADC), cerebral blood volume (CBV), and follow-up CE-T1WI.

parameters were consistent across all sequences, with a slice thickness of 5 mm, inter-slice gap of 1 mm, and field of view (FOV) of 220 mm × 220 mm.

DWI was conducted in the axial plane using a spin echo echo-planar sequence prior to contrast material injection. The imaging parameters included TR/TE = 8200/102 msec, number of excitations (NEX) = 2.0, slice thickness = 5 mm, inter-slice gap = 1 mm, and FOV = 220 × 220 mm, with a scan time of 1 min and 32 s. The b values used were 0 and 1000 s/mm^2, with diffusion gradients encoded in three orthogonal directions to generate three sets of diffusion-weighted images.

DSC-PWI was performed using a gradient-recalled T2*-weighted echo-planar imaging sequence. The imaging parameters included TR/TE = 1000–1250/54 msec, flip angle = 35°, slice thickness = 5 mm, inter-slice gap = 1 mm, NEX = 1.0, and FOV = 220 × 220 mm. During the first three phases, images were acquired before the injection of the contrast material to establish a precontrast baseline. For the fourth phase, a bolus of gadobenate dimeglumine (Gd-BOPTA) at a dose of 0.1 mmol/kg of body weight and a rate of 5 mL/s was injected intravenously using an MR-compatible power injector. Following the contrast injection, a 20.0 mL bolus of saline was administered at the same rate. A total of 1200 images were obtained over 20 sections and 60 phases in 1 min and 36 s. Some patients underwent dynamic contrast-enhanced MRI (DCE-MRI) before completing the DSC-PWI examination.

2.3. Image processing

Image processing was conducted using an offline Siemens syngo B19 workstation. The ADC map was automatically generated using Siemens Dynamic ADC software. DSC-PWI data were processed using Siemens Perfusion MR software. Initially, raw images were imported into the software, and an arterial inflow effect (AIF) map was delineated. Subsequently, the baseline and first-pass time range of the contrast agent were defined on the AIF map. T1 correction was then applied using the Perfusion MR software. Finally, hemodynamic parametric maps, including cerebral blood volume (CBV), cerebral blood flow (CBF), and mean transit time (MTT) maps, were reconstructed.

Preoperative multiparametric MR images and post-recurrence T1WI images were coregistered and projected onto preoperative T2WI images using Statistical Parametric Mapping (SPM) software based on MATLAB (Fig. 1). For the registration of ADC and DSC-PWI maps, DWI images with b value of 0 s/mm^2 and the first-phase DSC-PWI images were employed as the structural phase. The coregistered images were visually inspected and manually corrected by a neuroradiologist who was blinded to the results.

2.4. Image analysis

Following a previous study's protocol [16], a neuroradiologist (Z.X. with 12 years of experience in brain imaging), blinded to clinical and histopathological data, independently positioned five circular regions of interest (ROIs) in the NEPTRs on preoperative T2-FLAIR, ADC, and CBV maps for each patient, totaling 295 ROIs. Each ROI had a mean area of 36.21 mm^2 (range, 30–50 mm^2). Two ROIs were located in NEPTRs with future tumor recurrence, and three in NEPTRs without recurrence, referencing post-recurrence contrast-enhanced T1-weighted images (Fig. 1). Additionally, for each ROI, corresponding areas were measured in contralateral unaffected white matter deemed normal on both T2-and contrast-enhanced T1-weighted images. Subsequently, relative ratios of signal intensity of T2-FLAIR (rFLAIR), ADC (rADC), and CBV (rCBV) were calculated in NEPTR ROIs compared to contralateral unaffected white matter to account for individual variations (Fig. 1).

To evaluate inter- and intrareader variability of ROI measurements, another neuroradiologist (X.Y. with 7 years of experience in brain imaging) assessed multiparametric MRI in regions with and without future tumor recurrence, as well as in contralateral regions, in ten of 70 patients at various time points.

2.5. Statistical analysis

All parameters are presented as means ± standard deviation (SD). The inter- and intrareader reproducibility for all measurements was assessed using the intraclass correlation coefficient (ICC), with an ICC greater than 0.75 considered indicative of good agreement. Student's t-test was employed to compare rFLAIR, ADC, rADC, and rCBV values in the NEPTRs of GBM with and without future tumor recurrence. Receiver operating characteristic (ROC) curve analysis and logistic regression analysis were conducted to determine the diagnostic accuracy and optimal cutoff value of rFLAIR, ADC, rADC, rCBV, and their combined use for differentiating NEPTRs with future tumor recurrence from those without. Sensitivity, specificity, positive predictive value (PPV), negative predictive value (NPV), accuracy, and area under the curve (AUC) based on the optimal thresholds were calculated. The chosen cutoff values were those that

Table 1
Comparisons of rFLAIR, ADC, rADC, and rCBV values between the NEPTRs with and without future GBM recurrence (mean ± SD).

Parameters	NEPTRs with future tumor recurrence	NEPTRs without future tumor recurrence	*P* value
rFLAIR	1.74 ± 0.24	1.82 ± 0.21	0.002
ADC (×10^{-3} mm^2/s)	1.29 ± 0.27	0.64 ± 0.22	<0.001
rADC	1.87 ± 0.46	2.29 ± 0.43	<0.001
rCBV	1.16 ± 0.34	0.64 ± 0.22	<0.001

Note: NEPTRs, nonenhancing peritumoral regions; rFALIR, relative signal intensity of T2-weighted fluid-attenuated inversion recovery; ADC, apparent diffusion coefficient; rADC, relative apparent diffusion coefficient; rCBV, relative cerebral blood volume.

provided the optimal balance between sensitivity and specificity. Additionally, AUC comparisons for different quantitative variables were made using the Z-test. Statistical analysis was performed using Microsoft Excel 2013 (Microsoft, Redmond, Washington) and MedCalc statistical software (version 15.2.2, Ostend, Belgium), with P values less than 0.05 considered statistically significant.

3. Results

Strong intrareader agreements were achieved between two neuroradiologists for the measurements of rFLAIR, ADC, rADC, and rCBV values, with ICCs of 0.92, 0.95, and 0.92, respectively. Additionally, excellent interreader agreements were observed for different time points within one neuroradiologist for the measurement of the above parameters, with ICCs of 0.95, 0.96, and 0.94, respectively.

The rFLAIR, ADC, rADC, and rCBV values calculated in the NEPTRs of GBM with and without future tumor recurrence are summarized in Table 1. We observed that the rFLAIR value of the NEPTRs with future tumor recurrence was significantly lower than that of the NEPTRs without future tumor recurrence ($P = 0.002$). Both ADC and rADC values were significantly lower in the NEPTRs with future tumor recurrence compared to those without future tumor recurrence (both $P < 0.001$). Furthermore, the rCBV value of the NEPTRs with future tumor recurrence was significantly higher than that of the NEPTRs without future tumor recurrence ($P < 0.001$). Representative images are presented in Fig. 2.

The results of the ROC curve analysis for the individual use of rFLAIR, ADC, rADC, and rCBV values are presented in Table 2 and Fig. 3. Logistic regression analysis was employed to evaluate the combined performance of these parameters in differentiating the NEPTRs of GBM with future tumor recurrence from those without future tumor recurrence. As shown in Table 2 and Fig. 4, the combination of "rCBV + ADC" and "rCBV + ADC + rFLAIR" yielded comparable AUCs ($P = 0.934$), which were higher than those of the

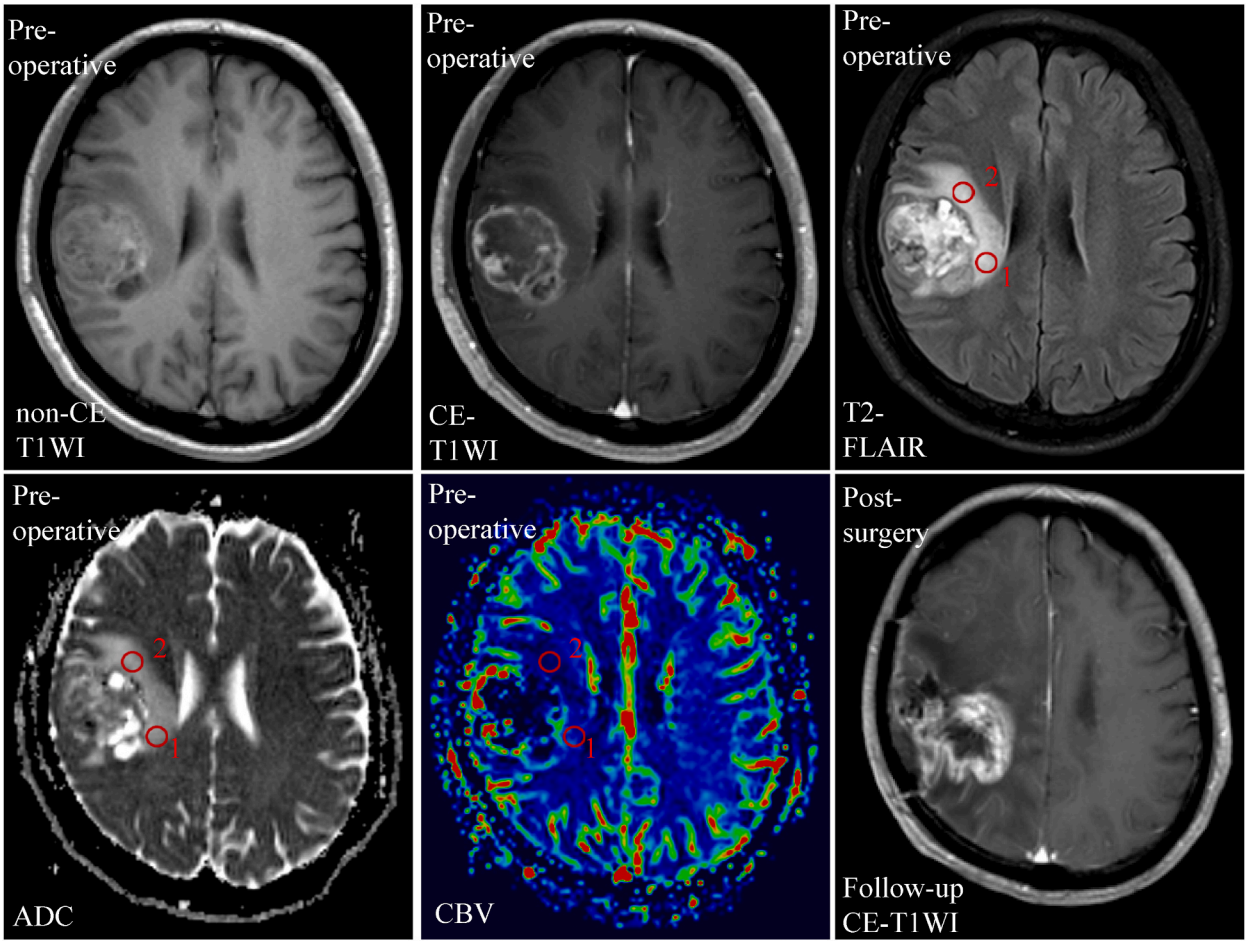

Fig. 2. Glioblastoma with future tumor recurrence in a 57-year-old man on preoperative and post-surgery MR images. ROIs 1 show areas with future tumor recurrence and ROIs 2 show areas without future tumor recurrence. The relative signal intensity of T2-weighted fluid-attenuated inversion recovery (rFLAIR), apparent diffusion coefficient (ADC), relative ADC, and relative cerebral blood volume (rCBV) measured from ROIs 1 and 2 are as follows: 2.12, 1.43 × 10^{-3} mm^2/s, 2.07, and 1.82, respectively, for ROI 1; 2.25, 1.57 × 10^{-3} mm^2/s, 2.28, and 0.76, respectively, for ROI 2. **Note:** CE-T1WI: contrast-enhanced (CE)-T1WI; T2-FLAIR: T2-weighted fluid-attenuated inversion recovery; ADC: apparent diffusion coefficient; CBV: cerebral blood volume.

Table 2
Predictive performance of single parameters (rFALIR, ADC, rADC and rCBV) and combined parameters (ADC + rFLAIR, rCBV + rFLAIR, rCBV + ADC, rCBV + ADC + rFLAIR) for identifying the NEPTRs with future tumor recurrence from those without tumor recurrence using receiver operating characteristic curve analysis and logistic regression analysis.

	TV	AUC	Sen	Spe	PPV	NPV	Acc
rFLAIR	1.68	0.599	75.7	44.9	52.7	77	63.1
ADC	1.41	0.798	76.8	72	64.5	82.5	73.9
rADC	2.01	0.756	74	66.9	59.6	79.2	69.5
rCBV	0.89	0.898	84.7	83.6	80.6	89.5	85.8
ADC + rFLAIR	–	0.798	76.8	72	64.5	82.5	73.9
rCBV + rFLAIR	–	0.903	85.3	83.9	78.3	89.8	84.7
rCBV + ADC	–	0.918	85.3	86.4	80.8	90	86.1
rCBV + ADC + rFLAIR	–	0.918	83.6	89	83.9	89.3	87.2

Note: NEPTRs, nonenhancing peritumoral regions; rFALIR, relative signal intensity of T2-weighted fluid-attenuated inversion recovery; ADC, apparent diffusion coefficient; rADC, relative apparent diffusion coefficient; rCBV, relative cerebral blood volume; TV, threshold value; AUC, area under the curve; Sen, sensitivity; Spe, specificity; PPV, positive predictive value; NPV, negative predictive value; Acc, accuracy.

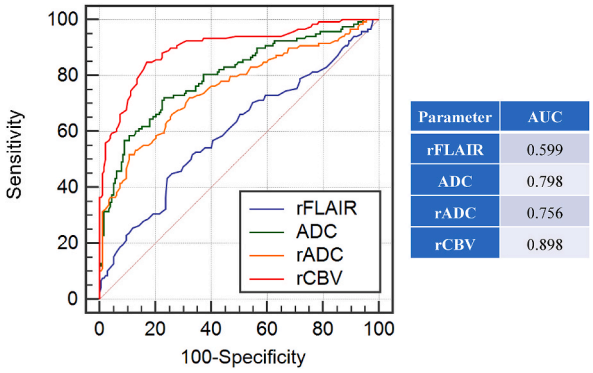

Fig. 3. Receiver operating characteristic curves of rFLAIR, ADC, rADC, and rCBV for identifying the nonenhancing peritumoral regions with future tumor recurrence from those without tumor recurrence. **Note:** rFLAIR: relative signal intensity of T2-weighted fluid-attenuated inversion recovery, ADC: apparent diffusion coefficient, rADC: relative ADC, rCBV: relative cerebral blood volume.

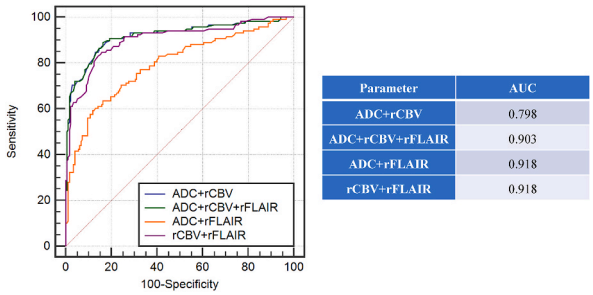

Fig. 4. Receiver operating characteristic curves of combined parameters, including "ADC + rFLAIR", "rCBV + rFLAIR", "rCBV + ADC", and "rCBV + ADC + rFLAIR", for identifying the nonenhancing peritumoral regions with future tumor recurrence from those without tumor recurrence. **Note:** rFLAIR: relative signal intensity of T2-weighted fluid-attenuated inversion recovery, ADC: apparent diffusion coefficient, rADC: relative ADC, rCBV: relative cerebral blood volume.

"ADC + rFLAIR" and "ADC + rCBV" models, as well as the most efficient single parameter, rCBV (all $P < 0.05$).

4. Discussion

In our study, we employed diagnostic parameters obtained from T2-FLAIR, DWI, and DSC-PWI to distinguish between NEPTRs of GBM with and without future tumor recurrence. Our results demonstrated that NEPTRs of GBM with future tumor recurrence displayed lower rFLAIR, ADC, and rADC values, but higher rCBV values. Furthermore, these parameters were effective in predicting NEPTRs at risk of future tumor recurrence at the baseline examination.

T2-FLAIR imaging, an essential component of brain MRI protocols, is highly sensitive to changes in water concentration and is thus

commonly used to assess the extent of non-enhancing tumor and edema [18]. Typically, clinical evaluation of the peritumoral T2-FLAIR high-signal-intensity region is limited to volumetric abnormalities [17]. Few studies have specifically investigated early changes in signal intensity on T2-FLAIR at baseline [11,13]. In a seminal study by Pope et al. [11], the signal intensity of microscopic GBM was slightly lower than that of pure edema on T2-FLAIR. Chang et al. [13] further demonstrated that decreased T2-FLAIR signal intensity was directly associated with the likelihood of tumor recurrence, emphasizing the predictive value of T2-FLAIR for future tumor recurrence in the NEPTRs of GBM. In our current study, we observed a significant decrease in rFLAIR in the NEPTRs with future tumor recurrence compared to those without, consistent with prior reports [11,13]. The reduction in T2-FLAIR signal intensity is believed to be inversely correlated with tumor cellularity [13], suggesting increased cell density in NEPTRs with future tumor recurrence due to infiltration by GBM tumor cells [19,20]. Therefore, our findings, in conjunction with previous research [11,13], suggest that a new signal increase on follow-up T2-FLAIR after gross total surgical resection may indicate progression of GBM infiltration.

The ADC value derived from DWI reflects the mobility of free water molecules within tissue and has been demonstrated to correlate with tumor cellularity [21]. ADC values are now widely used in tumor characterization, grading, and prognostication [22]. Several studies have suggested that ADC values in the peritumoral region may be useful for detecting neoplastic cell infiltration [23–26]. In our study, we observed that ADC and rADC values in the NEPTRs with future tumor recurrence were significantly lower than those in NEPTRs without recurrence, consistent with previous findings [13]. In that study, Chang et al. [13] analyzed ADC maps at the voxel level and noted that the extent of signal intensity decrease on ADC maps was directly proportional to the likelihood of tumor recurrence. In addition to increased cellularity, which also results in hyperintensity on T2-FLAIR imaging, active tumor proliferation by infiltrated tumor cells may be another factor contributing to the decrease in ADC values, significantly contributing to future local tumor recurrence in NEPTRs. Overall, our study suggests that a low ADC value in NEPTRs, indicative of tumor infiltration, may serve as a potential marker for predicting future tumor recurrence.

rCBV obtained from DSC-PWI is a valuable parameter for characterizing regional microvasculature and hemodynamics in brain tumors [27–29]. Previous studies have demonstrated the utility of rCBV in differentiating pseudo-progression and radiation necrosis from progression, as well as predicting treatment effects in gliomas [30–38]. However, to our knowledge, no previous study has utilized rCBV to predict NEPTRs at risk of future local tumor recurrence. Our study revealed that the rCBV value in NEPTRs with future tumor recurrence was significantly higher than in those without recurrence. Histopathologically, residual GBM tumor cells infiltrate slowly along existing vascular networks, disrupting endothelial tight junctions and facilitating leakage of gadolinium-based contrast agents through the blood-brain barrier [19,20]. Consequently, contrast agent leakage accumulates in the interstitial space, leading to an increase in rCBV value. Therefore, our findings suggest that preoperatively assessing rCBV values in NEPTRs may assist in early identification of regions at high risk of future local recurrence in patients with GBM.

Furthermore, all parameters, namely rFLAIR, ADC, rADC, and rCBV, demonstrated utility in predicting NEPTRs with future tumor recurrence compared to those without recurrence. Notably, according to ROC analyses, the sensitivity, specificity, and accuracy levels were significantly higher for perfusion parameters (rCBV accuracy, 85.8%) than for fluid-sensitive (rFLAIR accuracy, 63.1%) and diffusion parameters (ADC accuracy, 73.9%; rADC accuracy, 69.5%). Moreover, the combination of these promising diagnostic parameters collectively outperformed the individual use of rFLAIR, ADC, rADC, and rCBV in predicting NEPTRs with future tumor recurrence. Specifically, the "rCBV + ADC + rFLAIR" model exhibited the best predictive performance with an AUC of 0.918 and an accuracy of 87.2%. Thus, our study suggests that the combined utilization of multiparametric MRI, including T2-FLAIR, DWI, and DSC-PWI, can comprehensively provide physiopathologic information, potentially improving the characterization of subtle GBM tumor cell infiltration and predicting potential tumor recurrence at baseline.

Our study has several limitations. Firstly, the diagnosis of tumor recurrence in most cases was based on follow-up MRI images, lacking histopathological confirmation. Secondly, the absorption of the postoperative surgical cavity, along with the formation of surrounding scars and glial hyperplasia, may lead to some mismatches when registering post-recurrence images with preoperative multiparametric MRI images. To mitigate this, we employed ROI measurements in this study to minimize the impact of such inconsistent registration. Thirdly, enhanced lesions appearing 2 weeks after surgery may be attributed to the surgery itself, subacute infarcts, or residual tumor. In such cases, the combination of preoperative MRI images, DWI, and DSC-PWI can more accurately determine tumor changes. Finally, due to registration consistency and relatively small sample size, more advanced analysis methods such as radiomics and deep learning were not utilized in our study but should be considered in future investigations.

In conclusion, our study highlights the utility of T2-FLAIR, DWI, and DSC-PWI measurements in NEPTRs for early prediction of regions at risk of future tumor recurrence in patients with GBM. Specifically, higher rCBV emerges as a particularly effective parameter for predicting NEPTRs with future tumor recurrence. Furthermore, the combination of rFLAIR, ADC, and rCBV improves predictive performance, offering valuable insights into the likelihood of tumor recurrence at baseline.

Ethical statement

All procedures performed in the studies involving human participants were in accordance with the ethical standards of Fujian Medical University First Affiliated Hospital Ethical Committee (ethics approval number: 20221399), and with the 1964 Helsinki Declaration and its later amendments. Any patients whose images are included in this study have consented for their images to be published.

Funding

This study was supported by the National Natural Science Foundation of China (no 82071869), Fujian Provincial Health Technology Project (no. 2020GGA049), the Leading Project of the Department of Science and Technology of Fujian Province (no. 2020Y0025); Joint Funds for the Innovation of Science and Technology, Fujian Province (no. 2021Y9154).

Availability of data and materials

All data used in the generation of the results presented in this manuscript will be made available upon reasonable request from the corresponding author.

Data availability statement

Has data associated with your study been deposited into a publicly available repository?
No. Data will be made available on request.

CRediT authorship contribution statement

Zhen Xing: Writing – original draft, Methodology, Investigation, Data curation, Conceptualization. **Cong Wang:** Writing – review & editing, Writing – original draft, Investigation, Formal analysis, Data curation. **Wen Yang:** Methodology, Investigation. **Dejun She:** Writing – review & editing, Writing – original draft, Methodology, Investigation. **Xiefeng Yang:** Writing – review & editing, Writing – original draft, Methodology, Investigation, Formal analysis, Data curation. **Dairong Cao:** Writing – review & editing, Writing – original draft, Validation, Supervision, Methodology, Investigation, Funding acquisition, Formal analysis, Data curation, Conceptualization.

Declaration of competing interest

The authors declare that they have no known competing financial interests or personal relationships that could have appeared to influence the work reported in this paper.

Acknowledgement

None.

References

[1] A. Omuro, L.M. DeAngelis, Glioblastoma and other malignant gliomas: a clinical review, JAMA 310 (17) (2013) 1842–1850.
[2] R. Stupp, W.P. Mason, M.J. van den Bent, et al., Radiotherapy plus concomitant and adjuvant temozolomide for glioblastoma, N. Engl. J. Med. 352 (10) (2005) 987–996.
[3] R. Stupp, M.E. Hegi, W.P. Mason, et al., Effects of radiotherapy with concomitant and adjuvant temozolomide versus radiotherapy alone on survival in glioblastoma in a randomised phase III study: 5-year analysis of the EORTC-NCIC trial, Lancet Oncol. 10 (5) (2009) 459–466.
[4] T. Smets, T.M. Lawson, C. Grandin, A. Jankovski, C. Raftopoulos, Immediate post-operative MRI suggestive of the site and timing of glioblastoma recurrence after gross total resection: a retrospective longitudinal preliminary study, Eur. Radiol. 23 (6) (2013) 1467–1477.
[5] S. Lu, D. Ahn, G. Johnson, M. Law, D. Zagzag, R.I. Grossman, Diffusion-tensor MR imaging of intracranial neoplasia and associated peritumoral edema: introduction of the tumor infiltration index, Radiology 232 (1) (2004) 221–228.
[6] K. Petrecca, M.C. Guiot, V. Panet-Raymond, L. Souhami, Failure pattern following complete resection plus radiotherapy and temozolomide is at the resection margin in patients with glioblastoma, Journal of neuro-oncology 111 (1) (2013) 19–23.
[7] M. Weller, T. Cloughesy, J.R. Perry, W. Wick, Standards of care for treatment of recurrent glioblastoma–are we there yet? Neuro Oncol. 15 (1) (2013) 4–27.
[8] B.J. Gill, D.J. Pisapia, H.R. Malone, et al., MRI-localized biopsies reveal subtype-specific differences in molecular and cellular composition at the margins of glioblastoma, Proc. Natl. Acad. Sci. U.S.A. 111 (34) (2014) 12550–12555.
[9] Y. Li, R. Rey-Dios, D.W. Roberts, P.A. Valdes, A.A. Cohen-Gadol, Intraoperative fluorescence-guided resection of high-grade gliomas: a comparison of the present techniques and evolution of future strategies, World neurosurgery 82 (1–2) (2014) 175–185.
[10] A. Server, B. Kulle, J. Maehlen, et al., Quantitative apparent diffusion coefficients in the characterization of brain tumors and associated peritumoral edema, Acta Radiol. 50 (6) (2009) 682–689.
[11] W.B. Pope, J.H. Chen, J. Dong, et al., Relationship between gene expression and enhancement in glioblastoma multiforme: exploratory DNA microarray analysis, Radiology 249 (1) (2008) 268–277.
[12] K.M. McMillan, M. Ehtesham, C.B. Stevenson, M.L. Edgeworth, R.C. Thompson, R.R. Price, T2 detection of tumor invasion within segmented components of glioblastoma multiforme, J. Magn. Reson. Imag. 29 (2) (2009) 251–257.
[13] P.D. Chang, D.S. Chow, P.H. Yang, C.G. Filippi, A. Lignelli, Predicting glioblastoma recurrence by early changes in the apparent diffusion coefficient value and signal intensity on FLAIR images, AJR American journal of roentgenology 208 (1) (2017) 57–65.
[14] A. Di Costanzo, T. Scarabino, F. Trojsi, et al., Multiparametric 3T MR approach to the assessment of cerebral gliomas: tumor extent and malignancy, Neuroradiology 48 (9) (2006) 622–631.
[15] C.R. Durst, P. Raghavan, M.E. Shaffrey, et al., Multimodal MR imaging model to predict tumor infiltration in patients with gliomas, Neuroradiology 56 (2) (2014) 107–115.
[16] S. Bette, T. Huber, J. Gempt, et al., Local fractional anisotropy is reduced in areas with tumor recurrence in glioblastoma, Radiology 283 (2) (2017) 499–507.
[17] P.Y. Wen, D.R. Macdonald, D.A. Reardon, et al., Updated response assessment criteria for high-grade gliomas: response assessment in neuro-oncology working group, J. Clin. Oncol. 28 (11) (2010) 1963–1972.

[18] T. Kurki, N. Lundbom, S. Valtonen, Tissue characterisation of intracranial tumours: the value of magnetisation transfer and conventional MRI, Neuroradiology 37 (7) (1995) 515–521.
[19] S. Watkins, S. Robel, I.F. Kimbrough, S.M. Robert, G. Ellis-Davies, H. Sontheimer, Disruption of astrocyte-vascular coupling and the blood-brain barrier by invading glioma cells, Nat. Commun. 5 (2014) 4196.
[20] R.K. Jain, E. di Tomaso, D.G. Duda, J.S. Loeffler, A.G. Sorensen, T.T. Batchelor, Angiogenesis in brain tumours, Nat. Rev. Neurosci. 8 (8) (2007) 610–622.
[21] P.W. Schaefer, P.E. Grant, R.G. Gonzalez, Diffusion-weighted MR imaging of the brain, Radiology 217 (2) (2000) 331–345.
[22] E.R. Gerstner, A.G. Sorensen, Diffusion and diffusion tensor imaging in brain cancer, Semin. Radiat. Oncol. 21 (2) (2011) 141–146.
[23] E.J. Lee, K. terBrugge, D. Mikulis, et al., Diagnostic value of peritumoral minimum apparent diffusion coefficient for differentiation of glioblastoma multiforme from solitary metastatic lesions, AJR American journal of roentgenology 196 (1) (2011) 71–76.
[24] M. Kolakshyapati, R.B. Adhikari, V. Karlowee, et al., Nonenhancing peritumoral hyperintense lesion on diffusion-weighted imaging in glioblastoma: a novel diagnostic and specific prognostic indicator, J. Neurosurg. 128 (3) (2018) 667–678.
[25] I.C. Chiang, Y.T. Kuo, C.Y. Lu, et al., Distinction between high-grade gliomas and solitary metastases using peritumoral 3-T magnetic resonance spectroscopy, diffusion, and perfusion imagings, Neuroradiology 46 (8) (2004) 619–627.
[26] S. Lu, D. Ahn, G. Johnson, S. Cha, Peritumoral diffusion tensor imaging of high-grade gliomas and metastatic brain tumors, AJNR American journal of neuroradiology 24 (5) (2003) 937–941.
[27] P. Kickingereder, B. Wiestler, F. Sahm, et al., Primary central nervous system lymphoma and atypical glioblastoma: multiparametric differentiation by using diffusion-, perfusion-, and susceptibility-weighted MR imaging, Radiology 272 (3) (2014) 843–850.
[28] J.A. Guzman-De-Villoria, J.M. Mateos-Perez, P. Fernandez-Garcia, E. Castro, M. Desco, Added value of advanced over conventional magnetic resonance imaging in grading gliomas and other primary brain tumors, Cancer Imag. 14 (1) (2014) 35.
[29] C.Y. Ho, J.S. Cardinal, A.P. Kamer, S.F. Kralik, Relative cerebral blood volume from dynamic susceptibility contrast perfusion in the grading of pediatric primary brain tumors, Neuroradiology 57 (3) (2015) 299–306.
[30] R.F. Barajas Jr., J.S. Chang, M.R. Segal, et al., Differentiation of recurrent glioblastoma multiforme from radiation necrosis after external beam radiation therapy with dynamic susceptibility-weighted contrast-enhanced perfusion MR imaging, Radiology 253 (2) (2009) 486–496.
[31] I.E. Bennett, K.M. Field, C.M. Hovens, et al., Early perfusion MRI predicts survival outcome in patients with recurrent glioblastoma treated with bevacizumab and carboplatin, Journal of neuro-oncology 131 (2) (2017) 321–329.
[32] S. Blasel, A. Zagorcic, A. Jurcoane, et al., Perfusion MRI in the evaluation of suspected glioblastoma recurrence, J. Neuroimaging 26 (1) (2016) 116–123.
[33] Y.J. Choi, H.S. Kim, G.H. Jahng, S.J. Kim, D.C. Suh, Pseudoprogression in patients with glioblastoma: added value of arterial spin labeling to dynamic susceptibility contrast perfusion MR imaging, Acta Radiol. 54 (4) (2013) 448–454.
[34] J. Khalifa, F. Tensaouti, L. Chaltiel, et al., Identification of a candidate biomarker from perfusion MRI to anticipate glioblastoma progression after chemoradiation, Eur. Radiol. 26 (11) (2016) 4194–4203.
[35] P. Kickingereder, A. Radbruch, S. Burth, et al., MR perfusion-derived hemodynamic parametric response mapping of bevacizumab efficacy in recurrent glioblastoma, Radiology 279 (2) (2016) 542–552.
[36] K. Nael, A.H. Bauer, A. Hormigo, et al., Multiparametric MRI for differentiation of radiation necrosis from recurrent tumor in patients with treated glioblastoma, AJR American journal of roentgenology 210 (1) (2018) 18–23.
[37] R.N. Sawlani, J. Raizer, S.W. Horowitz, et al., Glioblastoma: a method for predicting response to antiangiogenic chemotherapy by using MR perfusion imaging–pilot study, Radiology 255 (2) (2010) 622–628.
[38] R. Singh, K. Kesavabhotla, S.A. Kishore, et al., Dynamic susceptibility contrast-enhanced MR perfusion imaging in assessing recurrent glioblastoma response to superselective intra-arterial bevacizumab therapy, AJNR American journal of neuroradiology 37 (10) (2016) 1838–1843.